Title page

The epigenetic landscape in purified myonuclei from fast and slow muscles

Mads Bengtsen[1], Ivan Myhre Winje[1], Einar Eftestøl [1,2,] Johannes Landskron[3], Chengyi Sun[2], Diana Domanska[4], Douglas P. Millay[2,5], Leonardo Meza-Zepeda[6], Kristian Gundersen[1]

1: Department of Biosciences, University of Oslo, Norway, 2: Division of Molecular Cardiovascular Biology, Cincinnati Children's Hospital Medical Center, Cincinnati, OH 45229, USA, 3: Centre for Molecular Medicine Norway, University of Oslo, Norway, 4: Department of Pathology, University of Oslo, Norway, 5: 5: Department of Pediatrics, University of Cincinnati College of Medicine, Cincinnati, OH 45229, USA, 6: Department of Core Facilities, Institute for Cancer Research, Oslo University Hospital, Oslo, Norway.

The sequence of authors is not finally decided.

Abstract

Muscle cells have different phenotypes adapted to different usage and can be grossly divided into fast/glycolytic and slow/oxidative types. While most muscles contain a mixture of such fiber types, we aimed at providing a genome-wide analysis of chromatin environment by ChIP-Seq in two muscle extremes, the almost completely fast/glycolytic extensor digitorum longus (EDL) and slow/oxidative soleus muscles. Muscle is a heterogeneous tissue where less than 60% of the nuclei are inside muscle fibers. Since cellular homogeneity is critical in epigenome-wide association studies we devised a new method for purifying skeletal muscle nuclei from whole tissue based on the nuclear envelope protein Pericentriolar material 1 (PCM1) being a specific marker for myonuclei. Using antibody labeling and a magnetic-assisted sorting approach we were able to sort out myonuclei with 95% purity. The sorting eliminated influence from other cell types in the tissue and improved the myo-specific signal. A genome-wide comparison of the epigenetic landscape in EDL and soleus reflected the functional properties of the two muscles each with a distinct regulatory program involving distal enhancers, including a glycolytic super-enhancer in the EDL. The two muscles are also regulated by different sets of transcription factors; e.g. in soleus binding sites for MEF2C, NFATC2 and PPARA were

enriched, while in EDL MYOD1 and SOX1 binding sites were found to be overrepresented. In addition, novel factors for muscle regulation such as MAF, ZFX and ZBTB14 were identified.

Introduction

The phenotype of skeletal muscle fibers differs as an adaption to different tasks. Some fibers have short twitches and rapid shortening velocities, but low endurance. Such fibers are used for short, but explosive external work (sprinting, throwing, stumbling etc.), but are easily fatigued and not very energy efficient. Other fibers have slow twitches and shortening velocities, but are fatigue resistant and have a low energy expenditure. Such fibers are used for tasks as keeping body and limb posture.

Fibers are generally classified into "fiber types" related to the predominant myosin heavy chain (MyHC) isoenzyme expressed in the cell. MyHC is the strongest molecular determinant of shortening speed. In rodents there are four different MyHC genes expressed in adult limb muscles namely *Myosin Heavy Chain 7* (*Myh7*), *Myh2*, *Myh1* and *Myh4* giving rise to the fiber types 1 (slowest), 2A, 2X and 2B (fastest) respectively. Partly coupled to the MyHC fiber type, the fibers display a spectrum of metabolic properties, from highly oxidative mitochondria-rich cells (type 1) to cells that are mainly glycolytic (type 2B). At the molecular level the different fiber types vary in isoform expression of various of proteins such as calcium pumps, oxygen related proteins and also sarcomere components other than MyHC.

Skeletal muscle is the most important metabolic organ in the body. It has been known for 40 years that differences in muscle fiber type composition is a strong individual predictor for developing metabolic syndrome (1). Metabolic syndrome is a cluster of conditions increasing the risk of heart disease, stroke and type 2 diabetes. These conditions include increased blood pressure, high blood sugar levels, excess body fat around the waist, and abnormal cholesterol or triglyceride levels. Metabolic syndrome is on the rise, and in several countries the prevalence is now over ¼ of the population (2). Epigenetic mechanisms like histone modifications and chromatin structure have been suggested to play an important role in the development of and predisposition for metabolic syndrome (3), but data supporting this is currently scarce.

Muscle fibers are post-mitotic and represent an interesting example of a balance between long term phenotypic stability yet malleability. Thus, phenotype can be changed by altering the pattern of electrical activity elicited in their sarcolemma by the motor neurons or electrical stimulation (4) and also by the mechanical stress created by contraction (5). These two external

61 factors are the major mechanistic foundations for the effects of exercise on muscle. However,
62 adult phenotype also dependents on the embryonal cell lineage and this origin limits the
63 adaptive ranges of training effects (6). The transition process has been studied in detail in rats
64 stimulated with electrical patterns mimicking extreme, but well-defined training (4). It appears
65 that some traits require very long-term treatment in order to be altered e.g. type 2 to type 1
66 transformations, which might take more than 3 months (7), in contrast changes within type 2 ,
67 i.e. 2B>2A>2X (8) and changes in metabolic and calcium sequestering enzymes can be altered
68 more rapidly (9). Suggesting that epigenetic mechanisms may play an important role in the
69 regulation of muscle plasticity (10, 11).

70 Recently the existence of a long term cellular muscle memory was demonstrated (12, 13), and
71 in addition to a permanently elevated number of myonuclei (14, 15) epigenetic mechanisms
72 might be involved (16). Epigenetic mechanisms might also be related to the observation that
73 some individuals seem to have less malleable muscles than others, i.e. exercise resistance (17-
74 19).

75 Since the overall chromatin environment and the modifications of the histones represent a form
76 of overreaching gene regulation mechanism with the potential of long-lasting stability (16, 20,
77 21), we set out to compare chromatin environment in an extremely fast/glycolytic muscle (the
78 m. extensor digitorum longus, EDL) and an extremely slow/oxidative muscle (the m. soleus) in
79 mice.

80 The majority of studies on epigenetics are on tissue culture cells, and less has been done on
81 tissue homogenates where results seem harder to interpret. In muscle, electron microscopy (22)
82 and a specific marker for myonuclei (22-24) has revealed that only approximately 40 – 50% of
83 the nuclei found in muscle tissue are myonuclei and since accounting for cellular heterogeneity
84 is critical in epigenome-wide association studies (25-28) we aimed at purifying the myonuclei
85 proper.

86 We recently reported that the nuclear envelope protein Pericentriolar material 1 (PCM1) can be
87 used as a specific light microscopy marker to discern the skeletal muscle myonuclei in both
88 rodents and humans (24), and we show here that this marker can be used to sort myonuclei to
89 >95% purity before a subsequent epigenetic analysis. Furthermore, we show that the
90 purification is necessary for the epigenetic landscape faithfully to reflect known features of

91 muscle function, and the results indicate that purification should be used in studies aimed at
92 elucidating the role of epigenetic mechanisms in muscle differentiation and plasticity.

93 Results

94 Purification of myonuclei allows a genome-wide analysis of muscle fiber specific
95 chromatin

96 *PCM1 labelling is specific for myonuclei isolated from the muscle tissue*

97 To remove interference from non-myofiber nuclei in the tissue, we took advantage of an
98 antibody against Pericentriolar material 1 (PCM1) which we have previously reported to
99 selectively label myonuclei in skeletal muscle fibers and not satellite cells or stroma cells (24,
100 29) (Fig. S1A).

101 To further prove the specificity of PCM1 for muscle myonuclei we used a transgenic mouse
102 model expressing Histone-2B coupled to GFP (H2B-GFP) under the control of the *skeletal*
103 *muscle Actin Alpha 1* (*ACTA1*) promoter giving specific expression of the fusion construct in
104 skeletal muscle fiber nuclei across fiber types (30). Single fiber analysis showed that H2B-GFP
105 and PCM1 labelling invariably colocalized (Fig 1A-B and Fig. S1C). In some cases, DAPI
106 labelled nuclei that were negative for both H2B-GFP and PCM1 were observed (arrows in Fig.
107 1D-E), probably representing non-myonuclei sticking to the fibers after isolation.

108 *PCM1 can be used to isolate myonuclei for subsequent analysis across species*

109 Flow cytometry analysis of nuclei from skeletal muscle displayed a 98.0 % overlap between
110 GFP and PCM1 labelling of the nuclei in the transgenic mouse line (Fig. 2A-F).

111 Analysis by flow cytometry of the nuclear composition in the tibialis anterior (TA) with mixed
112 fiber type composition and the two muscle extremes EDL and soleus with a fast and slow fiber
113 type composition, showed that the number of myonuclei varied from 40 % - 60 % with the
114 lowest number of myonuclei in the slow soleus (Fig. 2G-K), confirming that without sorting
115 roughly half of the nuclei isolated from muscle homogenates are from other cell types than
116 muscle fibers and might confound a genome-wide analysis aimed at this cell type.

117 To isolate the myonuclear fraction from the nuclei originating from the other cell types in the
118 tissue we used a magnetic-assisted sorting approach (Fig. 2G-J). Using this method, we were
119 able to isolate the myonuclei with a very high purity on an average of 95 % for all the three

different muscle type (Fig. 2G-K). The same high sorting purity was obtained when the three same muscle types from rat were analyzed (Fig. S2).

Purification of nuclei is required for a valid genome-wide analysis of the myo-specific epigenome

To investigate the importance of nuclear purification for epigenetic analysis of muscle cells we performed chromatin immunoprecipitation on the PCM1 purified nuclei followed by next-generation sequencing (ChIP-Seq) in soleus and EDL using an antibody against Histone H3 acetylated at Lysine 27 (H3K27ac), since its enrichment at promoter regions follows the transcriptional activity (31, 32), and compared it with H3K27ac signal in whole muscle(33). In the non-sorted material 12550 and 12243 promoters with H3K27ac peaks were identified in soleus and EDL respectively, and 27% and 14% of these did not have enrichment after purification (Fig. 3A-F). For both muscles, gene ontology analysis of the promoters with signal only in nuclei from the whole tissue showed they were related mainly to the immune system and angiogenesis (Fig. 3 D - E and Table S1). Extending the analysis to the full epigenomes for whole muscle tissue and the purified myonuclei for the two muscle types, showed similar results with enrichment for angiogenesis and blood related functions (Fig. S3 A-D and Table S1).

The effects of purification was well illustrated by the observation that genes used to identify non-muscle cells were found to be enriched for H3K27ac in non-purified nuclei, but not after the purification, e.g. *Fatty Acid Binding Protein 4* (*FABP4*) and *Endothelial Cell-Specific Molecule 2* (*ECSCR*) which are both used as marks for endothelia cells (34-38). Concerning fibroblasts, the two connective tissue genes, *Collagen* (*COL1A2*) (34, 39-41) and *Fibrillin 1* (*FBN1*) (42-44) were found to be enriched before purification but not after. Similar observations were made for the two leucocyte markers *Leukocyte Specific Transcript 1* (*LST1*) and *CD200 Molecule* (*CD200*) which play a role in the immune defense (45, 46). The purified myonuclei did not appear to contain nuclei from satellite cells. Thus, markers common for satellite cells such as *Apolipoprotein E* (*APOE*) (34, 35) and *C-X-C Motif Chemokine Receptor 4* (*CXCR4*) (47, 48), *Syndecan-3* (*SDC3*) (49-52) and the general progenitor and stem cell marker *CD34* (53-56) was enriched in the total nuclei from the whole tissue, but not after purification of the myonuclei.

The loci for genes classically known to be a part of the skeletal muscle cell such as the skeletal specific version of actin *ACTA1* and *Titin* (*TTN*) displayed enrichment in both the full tissue and PCM1-sorted population (Fig. 3G).

The epigenetic landscape in purified myonuclei from EDL and soleus reflects the differences in functional properties

To explore how the epigenome differed between the slow/oxidative soleus and fast/glycolytic EDL muscle cells, we focused on differentially enriched (DE) peaks between the two muscles using the histone modifications H3K4me3 and H3K27ac (Fold change (FC) >1.5 and a false discovery rate (FDR) < $1x10^{-2}$ and $1x10^{-7}$ for H3K4me3 and H3K27ac, respectively). We identified 719 H3K4me3 and 5309 H3K27ac DE peaks, corresponding to 7,6 % and 22,2 % of the sites, for each of these two histone modifications (Fig. 4 A-B). For H3K4me3 the majority of sites were localized around the promoter region, while for H3K27ac for most of the sites were found at distal regulatory enhancer regions (Fig. S4A-F). The higher number of DE peaks for H3K27ac suggesting that distal regulatory enhancers play important role in regulating the differences in function and phenotype, which is in line with previous observations of the epigenetic landscape between cell types from the same family (57, 58).

The epigenome reflects fiber type specific differences in contractile properties

The most fundamental way of classifying muscle fiber types has been the particular MyHC gene expressed in the fiber, but the sarcomeres differ with respect to other contractile proteins as well (59, 60). These features were reflected in the epigenome (Fig. 4C). Thus, the slowest MyHC isoform *Myh7* (coding for MyHC-1) on the mouse chromosome 14 had a larger enrichment in soleus compared to EDL, while the opposite was true for the fastest form *Myh4* (MyHC-2B) that is clustered with the other type 2 heavy chains on the mouse chromosome 11 (Fig. 4C). When considering all the four limb muscle MyHCs, the H3K27ac enrichment roughly resembled the histological fiber type distribution of the two muscles that we have found previously (61) (Fig. 4E). Similar differences in the epigenetic enrichment were found at the loci coding for the other sarcomeric proteins, such as the myosin light chains (*Myl1-3*) (Fig. 4D). The fast isoform of the gene coding for the contraction regulator *Myosin Binding Protein C2 (Mybpc2)* was enriched in the EDL, while paradoxically gene coding for the slow isoform *Myosin Binding Protein C1* (*Mybpc1*), was not in the soleus, however this is in agreement with RNA and protein levels for the isoform (62-64)

As expected, the loci containing the genes encoding developmental isoforms of the sarcomeric proteins *Myh3* (MyHC-emb) and MYH8 (MyHC-neo) (Fig. 4C and Fig. S5) or isoforms

specific for cardiac myocytes *Myh6* (MyHC- alpha) and *Troponin I3* (*Tnni3*/Troponin I), did not have any enrichment in these adult skeletal muscles (Fig. 4C).

The epigenome reflects fiber type specific differences the twitch speed

One of the major differences between different fiber types is the twitch duration, hence the EDL is a so called fast-twitch muscle and soleus a slow-twitch muscle. A major determinant of the twitch speed is the handling characteristics of Ca^{2+} (4, 60), and the expression level of relevant isoenzymes differs between different types of muscles (9, 41, 64, 65). Our data showed that this was also reflected at the epigenetic level such as for the, *ATPase Sarcoplasmic/Endoplasmic Reticulum Ca2+ Transporting* (*Atp2a*)*-1 and -2* (SERCA1 and -2), responsible for regulating the calcium levels in fast and slow muscle fibers respectively, *Casq1* and *-2* coding for the two calcium buffer proteins, *Calsequestrin 1* and *-2*, and *Pvalb* coding for the calcium binding protein Parvalbumin, highly specific for fast fibers (9) (Fig. 5).

For the genes coding for contractile and calcium proteins, the differences in the epigenome were not only restricted to the promoter regions, but also the inter- and intragenic areas with H3K27ac enrichment, such as the enhancer located inside the MyHC cluster at chromosome 11 between the long non-coding RNA *Linc-Myh* and *Myh2* (MyHC-2A) promoting fast glycolytic phenotype (66), and upstream enhancer regions at the slow isoforms of *Myh7* (MyHC-1) and *Atp2a2* (SERCA2) genes (67) (Fig. 4B and Fig. 5). Furthermore, we also identified the recently discovered fast phenotype specific enhancer located in the locus coding for the *Pvalb* (Parvalbumin) gene (33). This indicates the complexity and detailed regulation of the genes involved in contraction and calcium handling in the different muscle types.

The epigenome reflects fiber type specific differences in metabolic properties

Ontology analysis of the H3K27ac DE peaks showed that the regions are associated with genes involved in defining the metabolic properties for the two muscle types, such as lipid metabolism and mitochondria for soleus and muscle contraction and metabolism of hexose (e.g. sugar) for EDL (Fig. 6A-B and Table S2). Interestingly, a similar analysis carried out on whole tissue, identified fewer DE regions and only non-specific general functions (Fig. S4 G-H and Table S2). Again, underscoring the importance of sorting out the relevant nuclei from heterogenous tissues.

To further gain insight into how the epigenome adds to differences between the two types of muscles, we examined the differences in biological and signaling pathways using the dynamic

H3K27ac mark. The analysis identified that key factors and enzymes responsible for the metabolism and muscle size and -function have a different H3K27ac enrichment, both at promoters and distal regulatory enhances regions; such as Peroxisome proliferator-activated receptors (PPAR)- and the Fatty acid degradation pathways in soleus and the glycolysis and mitogen-activated protein kinase (MAPK) pathways in EDL (Table S3). Detailed analysis of the epigenetic landscape for two of the primary energy generating pathways, the fatty acid oxidation in soleus and glycolysis in EDL identified a complex epigenetic environment with several promoters and enhancers with a differently enrichment for the genes involved in the pathways (Fig. 6 C-E). For both the fatty acid oxidation pathway and glycolysis none of the involved genes were associated with DE regions for the opposite muscle type e.g. glycolysis enriched in soleus and fatty acid oxidation in EDL.

The epigenome indicates that the phenotype of fast/glycolytic and slow/oxidative muscles are determined by different regulatory networks

We sought to unravel the gene regulatory programs leading to the fast/glycolytic and slow/ oxidative phenotypes respectively, by using the myonuclei-specific DE H3K27ac regions in combination with DNase I hypersensitivity data for whole skeletal muscle (68, 69), which with a high resolution identifies where transcription factors and other proteins are bound to the chromatin (70). Motif enrichment analysis of the DE regions identified two distinct groups of transcriptional regulators for the two muscles. In soleus the SRY-Box Transcription Factor (SOX) and Nuclear Factor Of Activated T Cells (NFAT) motifs were the most overrepresented, while in EDL it was the E-boxes and Sine Oculis Homeobox Homolog (SIX) motifs (Table S4).

To consolidate and specify the analysis, we used the transcription factors from the motif enrichment analysis with the most significantly enriched promoter region and high quality motifs for each muscle. This revealed two distinct groups of transcription factors one for each muscle type; for soleus the factors such as SOX6, NFATC2, Myocyte Enhancer Factor 2C (MEF2C) and Peroxisome Proliferator-Activated Receptor Alpha (PPARA) were identified while for EDL factors such as Myogenic Differentiation1 (MYOD1), SIX1 and Zinc Finger and BTB Domain Containing 14 (ZBTB14) (Table S4). The transcription factors were identified to have 4530 and 4371 predicted binding sites connected to 464 and 392 DE promoter regions for soleus and EDL, respectively. Functional analysis of the genes connected to the transcription factors revealed that they are associated with central differences in the functional

246 phenotype between the two muscles (Table S5). Combining the information about factors,
247 genes and functions revealed distinct regulatory networks for the two muscles (Fig. 7). Though
248 different, they also share similarities, such as regulation of muscle contraction, but with a
249 different set of factors and genes involved (Fig. S6).
250

251 Discussion

252 We show that PCM1 selectively marks mature myonuclei in skeletal muscle, and that this
253 marker can be used to isolate the myonuclei from wild type fresh and frozen muscle samples.
254 This isolation method does not involve any enzymatic digestions or other treatments at elevated
255 temperatures, thereby preserving the native state of the epigenome. Furthermore, the method
256 relies on magnetic sorting, which simplifies the procedure. The sorting is important since only
257 less than 60% of the cell nuclei in muscle tissue are myonuclei (22, 24), and the sorting excluded
258 the large fraction of nuclei from satellite cells and stroma cells such as connective tissue and
259 vascular cells. The epigenetic signature of individual genes is highly cell-specific Studies of
260 other heterogenous tissues have also concluded that accounting for cellular heterogeneity is
261 critical in epigenome-wide association studies (25-27). Mixed cell populations are prone to
262 increase the number of false negatives and positives (32, 71). This point has also been addressed
263 in skeletal muscle by mechanically isolating single fibers preceding transcriptome (41) and
264 methylome (72); reducing the signal arising from non-myogenic cells residing in the tissue.

265 When we compared myonuclei from the two extreme muscles soleus and EDL we found that
266 they had a large part of the epigenome in common. Important differences were found in
267 connection to genes coding for proteins involved in contraction, calcium handling and
268 metabolic pathways; reflecting differences at the transcriptional and protein level between
269 different fiber types (41, 64, 73-75).

270 In addition, we found differences in distal enhancers at the loci reflecting different regulatory
271 network in the fast and the slow muscle. The two MyHC loci provide interesting examples of
272 differences in such regional regulation. In both mice and man, the slow type 1 *Myh7* (MyHC-
273 1) gene is located on chromosome 14 head to tail with the cardiac isoform *Myh6* (MyHC-
274 1alpha), while the fast type 2 isoforms are clustered on a 300-600 kb segment in the order *Myh4*,
275 *Myh2* and *Myh4*, reflecting the order of increasing of shortening velocity, MyHC-2A-2X-2B)
276 on the mouse chromosome 11 (in humans 17) (76). Interestingly, during exercise, activity-

induced changes are relatively easily obtained within the different type 2 MyHCs of the gene cluster, while 1⇔2 transformation is harder, and cannot be obtained, except under extreme conditions (7).

In the fast locus an intergenic SIX1 responsive enhancer between *Myh3* (MyHC-emb) and non-coding RNA *Linc-Myh* are located. It drives the expression of the fast myosin through higher order chromatin interactions and locks the muscle fiber in fast-glycolytic phenotype (66). Furthermore, the enhancer regulates the *Linc-Myh*, that additional play a role in maintaining the fast phenotype, presumable through trans-induced mechanisms (66). This area which is one of the most differently enriched in our data for the glycolytic EDL, revealed several additional enhancer regions upstream and downstream of the *Linc-Myh*, further adding to the complexity of the locus. In muscle cell culture this area has been identified to be a part of a special group of enhancers known as super-enhancers (77). This group of enhancers are characterized by spanning several kb and being important for defining the identity of the cell (78-80). As one of the most enriched area in EDL, it suggests that the super-enhancer also plays a role in the adult glycolytic fiber *in vivo* and might stabilize fiber types and be an obstacle to transformations.

For the regulatory network several of the transcription factors are well known regulators of skeletal muscle phenotype and function, such as NFAT, SOX, SIX and MYOD1 (4, 60, 81). Interestingly our enriched factors are largely in agreement with a recent study, using an alternative approach to investigate the epigenetic regulatory environment in slow and fast muscles at the single nuclei level (82).

Other factors we identified, such as MAF BZIP Transcription Factors (MAF) and ZBTB14, is just recently described to have a role in muscle regulation at the gene level (82, 83). The latter is identified to be involved in regulation of metabolism, a function also assigned to the factor in our regulatory network. More specifically, it is found to be a negative regulator of the myokines *Interleukin 6* (*IL6*) and *Leukemia inhibitory factor* (*LIF*) by binding to the promoter regions of the two genes (83). We identified two additional factors, largely unexplored in skeletal muscle namely the Zinc Finger Protein X-Linked (ZFX) in EDL and Transcription Factor 7 Like (TCF7L2) in soleus, but both has previously been suggested to be a part of skeletal muscle specific regulatory networks (64, 84). On the molecular level the ZFX is identified to facilitate transcription through binding in the promoter regions just downstream of the transcription start sites of target genes (85). In the case of TCF7L2, it is found to regulate the

308 expression of the slow *Myh7* (MyHC-1) (86) and modulate the chromatin environment in
309 oxidative muscle tissue (87).

310 For the soleus it is notable that the transcription factors MEF2C, PPARA, SOX6 and NFATC2
311 are identified as they are known to influence muscle in the slow/oxidative direction (60, 88-
312 91). MEF2C is previously identified to be important for slow fiber development and for the
313 energy homeostasis in these (92, 93).

314 Interestingly, MEF2C and its family members are known to interact with co-regulators that are
315 capable in altering the epigenetic environment such as histone acetyl transferase P300 (94, 95)
316 and lysine methyltransferase Myeloid/lymphoid or Mixed-Lineage Leukemia 4 (MLL4). In the
317 latter case, the transcription factor together with its co-regulator establish an open chromatin
318 environment at active enhancers that enforces an oxidative/slow muscle phenotype e. g. by
319 regulating sarcomeric slow genes such as *Myh7* (MyHC-1) and *Tnnc1* (Troponin C1) through
320 enhancers located upstream of their respective promoters (67). MEF2C is also participating in
321 muscle activity-related calcium regulation, both by being activated by downstream signaling
322 pathways such as MAPK and calmodulin-dependent protein kinases (CaMK) (96-98), but also
323 through regulation of the genes participating in the signaling cascades (99-101). From the
324 cardiac tissue the transcription factor is found to regulate the expression of the slow
325 sarcoplasmic calcium pump, *Atp2a2* (SERCA2), through an enhancer region (102), a
326 connection also identified in our soleus network. This points towards an interesting conserved
327 regulatory mechanism between heart and skeletal muscle.

328 The transcription factors PPARA and Estrogen Related Receptor Beta (ESRRB) are mediating
329 fatty acid degradation and oxidative metabolism (73, 103, 104). Similar roles are known for
330 additional members of their respective families (105, 106). In the case of PPARA, it is
331 furthermore reported to control the expression of metabolic genes in response to changes in the
332 environment through distal enhancers (107) and to be involved in regulation of contraction
333 (108, 109).

334 For EDL it was notable that SIX1 and MYOD1 appeared since there is evidence that they drive
335 the phenotype in the fast/glycolytic direction (4, 110, 111). The SIX1 transcription factor is
336 reported to be an important regulator of key genes defining the fast-glycolytic phenotype where
337 it regulates genes mediating glycolysis (e.g. *Aldoa* (Aldolase A), *Pfkm* (Phosphofructokinase)
338 and *Eno3* (Enolase 3) and calcium homeostasis (*Pvalb* (Parvalbumin) (112, 113) in addition to

regulating the non-coding RNA *Linc-Myh* and its enhancer region (113). MYOD1 is found to be important for correct glycolytic fiber type specification and composition (111, 114). On the molecular level MYOD1 is known as a master regulator and is proposed to work as an organizer of enhancers (115, 116) In line with this it is known to recruit histone modifiers and co-regulators p300 and its homologue CBP to target sites (94, 117, 118).

A recent muscle cell differentiation study in cell culture, MYOD1 were identified to take part in the regulation of the super-enhancer inside the fast MyHC locus covering the *Linc-Myh* and its enhancer (119). Pointing towards an interesting collaboration at the locus between MYOD1 as a master regulator and the more specific role of SIX1 in locking the expression of the fast myosin genes (66) thereby promoting the glycolytic phenotype.

In summary we have shown that PCM1 can be used to isolate the myonuclei from the complex whole muscle tissue and that in order to get a clear and faithful representation of the whole epigenome, such sorting should be performed prior to analysis of nuclei from the complex muscle tissue. Comparison of the myo-specific epigenomes of the two muscle extremes soleus and EDL show as expected that the majority of the epigenome in common. The parts that differed were regulatory elements and genes related to contraction speed, twitch duration, and metabolism. In addition, our epigenetic analysis revealed that the two muscles have distinct regulatory networks associated with genes defining the disparate phenotype.

Materials and Methods

Materials and Methods

Animal procedures

Female NMRI and (28-31 gram) and Sprague Dawley rats weighing 210-260 g were used. Animals were kept at the animal facility at the Department of Biosciences or Department of Medicine, University of Oslo. Animals were housed with a 12 h light/dark cycle with ad libitum access to food and water. Before surgery, animals were sedated with 2 % isoflurane (506949, Forene, Abbot) in the air. Following deep anesthesia, the hind limb muscles extensor digitorum longus (EDL), soleus and tibialis anterior (TA) were surgically removed and directly frozen in liquid nitrogen and transferred to cryotubes before being stored at -80 °C. Animals were sacrificed by cervical dislocation while under deep anesthesia. The research was conducted in accordance with the Norwegian Animal Welfare Act of 20th December 1974. The Norwegian

Animal Research Committee approved all experiments before initiation. The Norwegian Animal Research Authority provided governance to ensure that facilities and experiments were in accordance with the Act, National Regulations of January 15th, 1996, and the European Convention for the Protection of Vertebrate Animals Used for Experimental and Other Scientific Purposes of March 18th, 1986.

The ACTA1^{rtTA}; TRE$^{H2B\text{-}GFP}$ mice were kindly provided by Dr. John McCarthy (University of Kentucky)(30). To induce H2B-GFP expression, 2-month old mice were fed chow supplemented with Dox (625ppm) for 1 week. The Dox chow was purchased from TestDiet (54057). All procedures with the ACTA1^{rtTA}; TRE$^{H2B\text{-}GFP}$ mice were approved by the Cincinnati Children's Hospital Medical Center's Institutional Animal Care and Use Committee.

Immunohistochemistry and imaging

For cross section tissue sectioning, immunohistochemical staining and subsequent image processing were performed as previously described (24).

For single fiber imaging; EDL muscles from the ACTA1^{rtTA}; TRE$^{H2B\text{-}GFP}$ mice were collected and incubated in high-glucose DMEM (HyClone Laboratories) with 0.3% collagenase type I (Sigma-Aldrich) at 37 °C for 40 minutes, then washed with PBS. Muscles were gently triturated using a glass pipette to loosen digested myofibers until they shed from muscle and fixed over-night in 1% paraformaldehyde. Fibers were then put in staining buffer (0.6% Igepal-CA-630, 5% BSA and 1% goat serum in PBS) for 1h at room temperature, followed by staining with an antibody against PCM1 (1:1000, HPA023370, Sigma Aldrich) in staining buffer over night at 4 °C with gentle agitation. Next day fibers were washed (3x 30 min in staining buffer), incubated for 3 hours with secondary antibody (Abcam #150083) at 4 °C with gentle agitation, washed 3x 30 min in staining buffer and mounted with Fluoromount-G with DAPI (SouthernBiotech #0100-20). For Figure 1D-E, fibers were imaged on a Nikon A1 R confocal system through NIS-Elements AR software (ver.5.10.01) with a 60x oil immersion objective with NA of 1.4, using a Galvano scanner. For Figure S1, fibers were imaged on a Nikon Eclipse Ti inverted microscope with a 20x air immersion objective.

Myonuclear Isolation

All samples and buffers were kept on ice during the procedure. The muscle was removed from the -80 °C freezer and transferred to -20 °C where it was minced into pieces of 1-2 mm before being transferred to gentleMACS M-tubes (Miltenyi Biotec) tubes kept on ice. The samples

were homogenized in 5 ml of lysis buffer (10 mM Tric-HCl pH 8.0 (cold adjusted), 5 mM $CaCl_2$, 3 mM MgAc, 2 mM EDTA, 0,5 mM EGTA) on a gentleMACS Dissociator (Miltenyi Biotec) using the default homogenization program *protein_01*. All buffers were supplemented with 5 mM Na-butyrate (Sigma Aldrich), 5 mM PMSF (Sigma Aldrich) and 1x protease inhibitor (Complete Protease Inhibitor Cocktail, Roche) immediately before use. Following homogenization, the lysate was diluted in 5 ml lysis buffer containing 0.4 % Triton-X100. Samples were mixed 10 times with a 1 ml pipette before being filtered through a 100 μm and 30 μm strainers (Falcon, Sigma Aldrich) to remove large aggregates. The homogenates were transferred to a 15 ml tube and centrifuged at 1000 g for 5 minutes in a centrifuge with a swing-out rotor at 5 °C. The pellet was resuspended in 1 ml nuclei staining buffer (5 % BSA wt/vol, 0.2 % IGEPAL–CA630, 1 mM EDTA in Dulbecco's Phosphate Buffered Saline (DPBS) pH 7.4) (120) containing an antibody against PCM1 (1:1000, HPA023370, Sigma Aldrich). Samples were incubated using a tumbler (40 rpm) for 1 hour at 6 °C. Then centrifuged for 5 minutes at 800 g at 5°C and the pellet was resuspended in 500 μl sorting buffer (1 % BSA wt/vol, 2 % skimmed milk powder (Sigma Aldrich), 1 mM EDTA in PBS pH 7.4) and spun down at 600 g at 5°C for 5 minutes at slow acceleration settings. The pellets were resuspended in 100 μl beads buffer consisting of 80 μl sorting buffer with 20 μl secondary Anti-rabbit IgG MicroBeads (Miltenyi Biotec) and incubated for 15 min in at 4 °C sorting buffer (900 μl). After incubation, the samples were centrifuged as above and wash once with Sorting buffer before resuspended in 1 ml of the same buffer and incubated for 5 minutes at a tumbler at 40 rpm at 6 °C. After incubation, the sample was carefully applied to a M column (Miltenyi Biotec), washed 3 times with 1 ml Sorting buffer and eluted with 1 ml Sorting buffer after removal from the magnet. The eluate was applied to another M column, washed again and eluted in 1 ml elution buffer (DPBS with 1 mM EDTA). The efficiency of sorting was determined by staining aliquots before and after myonuclear enrichment.

Chromatin immunoprecipitation

All buffers were supplemented with 5 mM Na-butyrate (Sigma Aldrich), 5 mM PMSF (Sigma Aldrich) and 1x protease inhibitor (Complete Protease Inhibitor Cocktail, Roche) immediately before use. Nuclei, approximately 300 000, were fixated with 1 % freshly prepared formaldehyde (Fisher Scientific) in DPBS for 2 min at room temperature. Reaction was stopped by adding glycine to a final concentration of 125 mM. After 5 minutes of incubation at RT, nuclei were transferred to ice and washed two times with ice cold DPBS and lysed in 130 μl sonication buffer (50 mM Tris-HCl pH 8.0 (cold adjusted), 1 mM EDTA, 0.1 % wt/vol SDS).

Samples were sonicated for 8 minutes (30 sec on/off cycles) using a Bioruptor Pico (Diagnode) yielding on average DNA fragments of 200 - 300 bp. Lysate was diluted in an equal volume of 2x RIPA buffer (20 mM Tris-HCl pH 8.0 (cold adjusted), 280 mM NaCl, 1 mM EDTA, 1 mM EGTA, 2 % Triton X-100, 0.2 % Na-deoxycholate, 0.1 % SDS), and adjusted to 800 μl with RIPA buffer (10 mM Tris-HCl pH 7.5 (cold adjusted), 140 mM NaCl, 1 mM EDTA, 0.5 mM EGTA, 1 % Triton X-100, 0.1 % Na-deoxycholate, 0.1 % SDS). Samples were centrifuged at 12 000 g for 10 minutes and the supernatant was transferred to new tubes and precleared with 10 μl Protein A Dynabeads (Invitrogen) for 1 hour. For each sample, ChIP assays were performed in parallel with antibodies directed against H3K27ac (C15410196, Diagnode) and H3K4me3 (C15410003, Diagnode) or IgG (Kch-504-250, Diagnode). Antibodies (2 μg per sample) were incubated 10 μl to Protein A Dynabeads for two hours on a rotator at 40 rpm at 6 °C. Beads were transferred to PCR-tubes and captured with a magnetic rack followed by addition of 150 μl ChIP ready chromatin. Samples were incubated at 40 rpm on a tube rotator overnight at 40 rpm at 6 °C. Next morning, the supernatant was removed and the beads was washed with 100 μl RIPA-buffer, followed by a washing step with high salt RIPA (20 mM Tris-HCl (cold adjusted) pH 8.0, 500 mM NaCl, 1 mM EDTA, 1 mM EGTA, 2% Triton X-100, 0.2 % Na-deoxycholate, 0.1 % SDS) and a washing step with LiCl buffer (20 mM Tris-HCl pH 8.0 (cold adjusted), 250 mM LiCl, 1 mM EDTA, 1 mM EGTA, 2 % Triton X-100, 0.2 % Na-deoxycholate, 0.1% SDS) and once with TE-buffer (20 mM Tris-HCl pH 8.0). All washing steps were being performed for 5 minutes using a rotor at 40 rpm and at 6 °C, with the exception of the TE-buffer washing steps which was carried out at room temperature. After the final washing step, the beads were resuspended in 96 μl elution buffer (20 mM Tris-HCl pH 7.5, 5 mM EDTA, 50 mM NaCl, 1 % SDS) and incubated on heating block at 37˚C. After one hour, 1 μl Proteinase K (20 µg/ul) was added to each sample and incubated for one hour at 50˚C followed by 4 hours at 68˚C on thermoshaker at 1200 rpm. ChIP DNA was purified with Zymo ChIP DNA Clean & Concentrator kit in 10 μl (Zymo Research).

Flow cytometry

For flow cytometry analysis nuclei were isolated as described above. For the ACTA1^{rtTA}; TRE$^{H2B\text{-}GFP}$ TA muscles were excised, minced with a razor, and homogenized in PBS containing 0.25 M sucrose and 1% BSA using an Ultra-Turrax T25. The homogenate was then incubated for 5 minutes with addition of Triton-X100 to a final concentration of 0.36 % at 4 °C. Samples were filtered through a 100 µm strainer, then filtered again through a 40 µm strainer. The nuclei pellet was collected after centrifugation (3000 ×g for 5 minutes at 4 °C), and

resuspended in sorting buffer (2 % BSA/ PBS). PCM1 (HPA023370, Sigma Aldrich) staining was performed on ice for 1 hour (1:1000). After washing, samples were stained with the secondary antibody Alexa Fluro 647 anti-rabbit IgG (A32795, Invitrogen)(1:1000) for 30 minutes in combination with Hoechst 33342 (Life Technologies) added 1:5000. Stained samples were analysed on a BD FACSCanto II or a BD LSRII. Data analysis was performed utilizing BD FACS Diva, FlowJo and Kaluza.

Next-generation sequencing

Libraries for next-generation sequencing (NGS) were created with the Swift Accel-NGS 2S Plus DNA Library Kit (Swift Biosciences) following the recommendations from the manufacturer with the exception that the ratio of beads and PEG was 1.5 and 1.3 in step Repair step I and II, respectively and amplified with 12 PCR cycles. The libraries were sequenced on a HiSeq 2500 40 bp paired-end, Illumina at the Norwegian Sequencing Centre.

Bioinformatics analysis

The ChIP-Seq reads were trimmed with TrimGalore (121) and mapped to the mouse genome (mm9) using BWA (122). Duplicated and low-quality reads were removed (q >10) using Samtools (123). Enriched regions were identified with PePr using the three biological replicates for each histone modification over the respective input samples using the following parameters --sharp for peak calling and a p-value threshold on 0.05 (124). Differently enriched regions were identified using PePr --diff with the biological replicates over their respective input for each sample and using threshold on foldchange 1.5 or above and a FDR-value on $1x10^{-5}$ for H3K4me3 and $1x10^{-7}$ for H3K27ac or below in addition to intersect with peaks identified in their respective samples.

For gene annotation UCSC Known Genes (mm9) with an ensemble id were used. Promoters were defined as upstream of 750 bp and downstream of 250 bp of transcription start site (TSS). For visualization samples were normalized to input and BigWig files were created as described in (125). Heatmap of ChIP-Seq signals were created with deepTools version 3.3.0 (126) Gene ontology analyzes of DE peaks were performed with GREAT v. 4.04 (127) using single closets gene while pathway analysis was conducted with David v. 6.8 (128, 129). Redundancy reduction was performed with ReViGO (130).

Regulatory networks were visualized with Cytoscape (131). DNase I hypersensitive enrichment data for mouse skeletal muscle were obtained from (68, 69). For the analysis, only middle point of DNase I enriched areas -/+ 100 bp inside the myo-specific H3K27ac enriched areas for Soleus and EDL were used. Motif enrichment analysis was conducted with AME Version 5.0.4

(132) using high quality motifs from human and mouse and threshold on FDR < $1x10^{-5}$. For factors with similar motif, the factor with the most significant H3K27ac enrichment at the promoter region (FDR < $1x10^{-15}$) was included. Functional annotation clustering of enriched promoters was conducted with David v. 6.8 (128, 129).

Data have been made publicly available under GEO (accession number GSExxxxxx)

ACKNOWLEDGEMENTS

We would like to thank Inga Juvkam for technical assistance. Bioinformatics analyses were performed at the Abel Cluster (project nn9540k), owned by the University of Oslo and the Norwegian metacenter for High-Performance Computing (NOTUR).

Funding:

The Research Council of Norway (grant 240374), the Wedel Jarlsberg Foundation and the Nansen Foundation. The work in the Millay laboratory was funded by grants to D.P.M. from the Children's Hospital Research Foundation, Pew Charitable Trusts, and National Institutes of Health (R01AR068286, R01AG059605).

Conflict of interest statement:

None declared.

Figure legends:

Fig. 1: PCM1 selectively labels myonuclei in isolated single fibers. A) Max intensity Z projection of single fiber from transgenic mouse expressing the H2B-GFP (Green) construct under the control of ACTA1 stained against PCM1 (magenta). Counterstained with DAPI to visualize DNA (Blue) D) Arrow: nucleus negative for both PCM1 and H2B-GFP. Scale bar 50 μm E) High resolution image of single fiber showing GFP positive and negative nuclei. Scale bar 10 μm.

Fig. 2: **PCM1 can be used to isolate the myonuclei population from whole skeletal muscle tissue.** A) Nuclei from whole muscle lysate stained with PCM1 antibody (green) and Hoechst to visualize DNA (blue), Scale bar 20 μm. B) Representative scatterplot showing identification of single nuclei from skeletal muscle tissue by flow cytometry. C-D) Representative scatterplot of nuclei labeled with PCM1 and IgG, respectively. E) Representative scatterplot of co-localization between nuclei expressing H2B-GFP and positive for PCM1 in tibialis anterior (TA) from mouse expressing the H2B-GFP construct under the control of ACTA1, analyzed by flow cytometry. F) Co-localization between PCM1 and GFP positive nuclei in TA in the transgenic mouse model (n=3), error bare SEM. G) Workflow used to isolate the myo-specific nuclei from skeletal muscle. H-J) Representative histograms of nuclear distribution and magnetic sorting efficiency for the three muscles TA, EDL and soleus (SOL) from mice by flow cytometry. K) Quantification of nuclear distribution in full tissue (n=3). J) Quantification of sorting efficiency (n=3).

Fig. 3: **The epigenome of whole tissue is different from the myonuclei specific**. A-B) Comparison of H3K27ac enrichment at gene promoter regions from whole muscle tissue and PCM1 isolated myonuclei for soleus and EDL respectively. C-D) Gene ontology enrichment analysis of promoter regions with H3K27ac enrichment specific for whole muscle tissue (grey). See Table S1 for full list. E-F) Heatmaps showing H3K27ac enrichment at the promoter regions in A-B -whole tissue and sorted myonuclei, in soleus and EDL respectively. G) H3K27ac enrichment in whole tissue and sorted myonuclei for loci used to define cellular populations.

Fig. 4:The differences in physiology are also present at the epigenetic leve1. A-B) Venn-diagrams showing number of peaks with similar or different enrichment for the histone marks H3K27ac and H3K4me3 in myonuclei. C) ChIP-Seq profiles of the myo-specific H3K4me3 and H3K27ac enrichment at the genomic loci containing the genes coding for the contractile proteins defining the muscle types: the main myosin types at the MyHC locus at chromosome 11 (*Myh1,-2,-4*) coding for the fast isoforms as well as the embryonically expressed *Myh3* and the non-coding RNA *Linc-Myh*, the slow *Myh7* gene at chromosome 14, and the Troponin genes the slow *Tnnt1* and the fast *Tnnt3* at chromosome 7. D) Relative H3K27ac enrichment for peaks overlapping the promoter regions for the four-principle myosin heavy chains (*Myh1,2,4 and -7*) and protein level for the corresponding proteins assessed by immunohistochemistry (MyHC1, MyHC-2A, -2B and -2X). E) Fold change differences in SOL/EDL in the H3K27ac enrichment in peaks overlapping the promoter region for the genes coding for phenotype defining contractile proteins. Gene names in black, protein names in grey. No significant difference in the enrichment for *Mybpc1*

Fig. 5: Genes involved in the calcium signaling have a diverse epigenome A) ChIP-Seq profiles of the myo-specific H3K4me3 and H3K27ac enrichment at the genomic loci containing the genes coding for calcium signaling proteins: *ATPase Sarcoplasmic/Endoplasmic Reticulum Ca2+ Transporting (Atp2a1,*SERCA1) at chromosome 7, *Atp2a2* (SERCA2) at chromosome 5, *Calsequestrin 1* (*Casq1*) at chromosome 1*, Calsequestrin 2* (*Casq2*) at chromosome 3 and *Parvalbumin* (*Pvalb*) at chromosome 15, in soleus and EDL, respectively.

Fig. 6. The epigenomes of the muscle extremes are enriched for different metabolic profiles. A-B) Plot of enriched gene ontologies for myo-specific differently H3K27ac peaks enrichment in soleus and EDL, respectively. The ontologies are shown after redundancy reduction with ReViGO by functional similarity. Terms are clustered in the semantic space by their similarity, without intrinsic meaning to the semantic space units. Selected terms for each cluster are shown, see Table S2 for full list. Ontologies identified with GREAT using closest promoter. C) ChIP-Seq profiles of the myo-specific H3K4me3 and H3K27ac enrichment in soleus and EDL, for two loci with differently enrichment, encoding *Fatty acid translocase* (*Cd36/Fat*) at chromosome 5 and *Lactate dehydrogenase A* (*Ldha*) at chromosome 7, respectively. D-E) Schematic representation showing the genes encoding the enzymes involved in the fatty-acid oxidation and glycolysis, respectively. Genes with a differently enriched H3K27ac promoter colored in red and blue for soleus and EDL, respectively. Grey denoted no difference in enrichment. Differently enriched alternative promoters and enhancer regions are shown as nodes with relative distance to the primary promoter region. Color code denotes the FDR significance level of the differential enrichment between the two muscle types.

***Fig.* 7**: **The muscle extremes are enriched for different regulatory networks.** Transcriptional regulatory network for soleus (A) and EDL (B). Top row constitutes of transcription factors with motif enriched in DE H3K27ac peaks, the middle of associated genes with a DE promoter (< 100 kb). The last row shows biological functions assigned to the genes. Edges between transcription factor and genes represent identification of predicted binding site for the respective transcription factor site and the gene it is connected to. Edges between genes and biological function denotes the functional properties assigned to the gene. Transcription factor motifs were identified with AME using high-quality motifs from human and mouse FDR < $1x10^{-5}$. For factors with similar motifs, the factor with the most significantly enriched promoter in the respective muscle type was used. Biological functions represent functional annotation clusters associated with the differential enriched genes (Clusters identified with David using an enrichment score >2.2 for the clusters and a p-value and fold change for the ontologies at < $5x10^{-2}$ and >3, respectively). Network visualized with Cytoscape. For the sake of clarity, only selected genes, with their most significant edge

to each transcription factor, and terms are shown. See Table S4 for the full names of transcription factor of factors and motifs and Table S5 for functional annotation clusters and genes.

References

1. Juhlin-Dannfelt A, Frisk-Holmberg M, Karlsson J, Tesch P. Central and peripheral circulation in relation to muscle-fibre composition in normo- and hyper-tensive man. Clin Sci (Lond). 1979;56(4):335-40.
2. Saklayen MG. The Global Epidemic of the Metabolic Syndrome. Curr Hypertens Rep. 2018;20(2):12.
3. Kirchner H, Osler ME, Krook A, Zierath JR. Epigenetic flexibility in metabolic regulation: disease cause and prevention? Trends Cell Biol. 2013;23(5):203-9.
4. Gundersen K. Excitation-transcription coupling in skeletal muscle: the molecular pathways of exercise. Biol Rev. 2011;86(3):564 - 600.
5. Eftestøl E, Egner IM, Lunde IG, Ellefsen S, Andersen T, Sjåland C, et al. Increased hypertrophic response with increased mechanical load in skeletal muscles receiving identical activity patterns. Am J Physiol-cell Ph. 2016;311(4):ajpcell.00016.2016.
6. Eken T, Gundersen K. Electrical stimulation resembling normal motor-unit activity: Effects on denervated fast and slow rat muscles. J Physiol. 1988;402(651):651-69.
7. Windisch A, Gundersen K, Szabolcs MJ, Gruber H, Lomo T. Fast to slow transformation of denervated and electrically stimulated rat muscle. J Physiol. 1998;510(Pt 2):623-32.
8. Gorza L, Gundersen K, Lomo T, Schiaffino S, Westgaard RH. Slow-to-fast transformation of denervated soleus muscles by chronic high-frequency stimulation in the rat. J Physiol. 1988;402:627-49.
9. Gundersen K, Leberer E, Lomo T, Pette D, Staron RS. Fibre types, calcium-sequestering proteins and metabolic enzymes in denervated and chronically stimulated muscles of the rat. J Physiol. 1988;398:177-89.
10. Pandorf CE, Haddad F, Wright C, Bodell PW, Baldwin KM. Differential epigenetic modifications of histones at the myosin heavy chain genes in fast and slow skeletal muscle fibers and in response to muscle unloading. Am J Physiol Cell Physiol. 2009;297(1):C6-16.
11. Baldwin KM, Haddad F, Pandorf CE, Roy RR, Edgerton VR. Alterations in muscle mass and contractile phenotype in response to unloading models: role of transcriptional/pretranslational mechanisms. Front Physiol. 2013;4:284.
12. Bruusgaard JC, Johansen IB, Egner IM, Rana ZA, Gundersen K. Myonuclei acquired by overload exercise precede hypertrophy and are not lost on detraining. Proc Natl Acad Sci U S A. 2010;107(34):15111-6.
13. Egner IM, Bruusgaard JC, Eftestol E, Gundersen K. A cellular memory mechanism aids overload hypertrophy in muscle long after an episodic exposure to anabolic steroids. J Physiol. 2013;591(Pt 24):6221-30.
14. Bruusgaard JC, Gundersen K. In vivo time-lapse microscopy reveals no loss of murine myonuclei during weeks of muscle atrophy. J Clin Invest. 2008;118(4):1450-7.
15. Lee H, Kin K, Kim B, Shin J, Rajan S, Wu J, et al. A cellular mechanism of muscle memory facilitates mitochondrial remodeling following resistance training. J Physiol. 2019;DOI: 10.1113/JP275308.
16. Seaborne RA, Strauss J, Cocks M, Shepherd S, O'Brien TD, Someren KAv, et al. Human Skeletal Muscle Possesses an Epigenetic Memory of Hypertrophy. Sci Rep-uk. 2018;8(1):1898.

17. Malin SK, Liu Z, Barrett EJ, Weltman A. Exercise resistance across the prediabetes phenotypes: Impact on insulin sensitivity and substrate metabolism. Rev Endocr Metab Disord. 2016;17(1):81-90.
18. Schiaffino S, Reggiani C, Akimoto T, Blaauw B. Molecular Mechanisms of Skeletal Muscle Hypertrophy. J Neuromuscul Dis. 2020.
19. Reggiani C, Schiaffino S. Muscle hypertrophy and muscle strength: dependent or independent variables? A provocative review. Eur J Transl Myol. 2020;30(3):9311.
20. Sen P, Shah PP, Nativio R, Berger SL. Epigenetic Mechanisms of Longevity and Aging. Cell. 2016;166(4):822-39.
21. Sharples AP, Stewart CE, Seaborne RA. Does skeletal muscle have an 'epi'-memory? The role of epigenetics in nutritional programming, metabolic disease, aging and exercise. Aging Cell. 2016;15(4):603 - 16.
22. Schmalbruch H, Hellhammer U. The number of nuclei in adult rat muscles with special reference to satellite cells. The Anatomical record. 1977;189(2):169 - 75.
23. Schmalbruch H, Hellhammer U. The number of nuclei in adult rat muscles with special reference to satellite cells. Anat Rec. 1977;189(2):169-75.
24. Winje IM, Bengtsen M, Eftestøl E, Juvkam I, Bruusgaard JC, Gundersen K. Specific labelling of myonuclei by an antibody against Pericentriolar material 1 (PCM1) on skeletal muscle tissue sections. Acta physiologica (Oxford, England). 2018;9(4):e13034.
25. Michels KB, Binder AM, Dedeurwaerder S, Epstein CB, Greally JM, Gut I, et al. Recommendations for the design and analysis of epigenome-wide association studies. Nat Methods. 2013;10(10):949 - 55.
26. Jaffe AE, Irizarry RA. Accounting for cellular heterogeneity is critical in epigenome-wide association studies. Genome Biol. 2014;15(2):R31.
27. Cheow LF, Courtois ET, Tan Y, Viswanathan R, Xing Q, Tan RZ, et al. Single-cell multimodal profiling reveals cellular epigenetic heterogeneity. Nat Methods. 2016;13(10):833-6.
28. Gundersen K, Bruusgaard JC. Nuclear domains during muscle atrophy: nuclei lost or paradigm lost? J Physiol. 2008;586(11):2675-81.
29. Winje IM, Sheng X, Hansson KA, Solbrå A, Tennøe S, Saatcioglu F, et al. Cachexia does not induce loss of myonuclei or muscle fibers during xenografted prostate cancer in mice. Acta physiologica (Oxford, England). 2018:e13204.
30. Iwata M, Englund DA, Wen Y, Dungan CM, Murach KA, Vechetti IJ, et al. A novel tetracycline-responsive transgenic mouse strain for skeletal muscle-specific gene expression. Skeletal muscle. 2018;8(1):1 - 8.
31. Karlić R, Chung H-R, Lasserre J, Vlahovicek K, Vingron M. Histone modification levels are predictive for gene expression. Proc National Acad Sci. 2010;107(7):2926-31.
32. Preissl S, Schwaderer M, Raulf A, Hesse M, Grüning BA, Köbele C, et al. Deciphering the Epigenetic Code of Cardiac Myocyte Transcription. Circ Res. 2015;117(5):413-23.
33. Ramachandran K, Senagolage MD, Sommars MA, Futtner CR, Omura Y, Allred AL, et al. Dynamic enhancers control skeletal muscle identity and reprogramming. PLoS biology. 2019;17(10):e3000467.
34. De Micheli AJ, Spector JA, Elemento O, Cosgrove BD. A reference single-cell transcriptomic atlas of human skeletal muscle tissue reveals bifurcated muscle stem cell populations. Skelet Muscle. 2020;10(1):19.
35. Rubenstein AB, Smith GR, Raue U, Begue G, Minchev K, Ruf-Zamojski F, et al. Single-cell transcriptional profiles in human skeletal muscle. Sci Rep. 2020;10(1):229.

671 36. Elmasri H, Ghelfi E, Yu CW, Traphagen S, Cernadas M, Cao H, et al. Endothelial
672 cell-fatty acid binding protein 4 promotes angiogenesis: role of stem cell factor/c-kit pathway.
673 Angiogenesis. 2012;15(3):457-68.
674 37. Huminiecki L, Bicknell R. In Silico Cloning of Novel Endothelial-Specific Genes.
675 Genome Res. 2000;10(11):1796-806.
676 38. Verissimo AR, Herbert JMJ, Heath VL, Legg JA, Sheldon H, Andre M, et al.
677 Functionally defining the endothelial transcriptome, from Robo4 to ECSCR. Biochem Soc T.
678 2009;37(Pt 6):1214-7.
679 39. Gillies AR, Lieber RL. Structure and function of the skeletal muscle extracellular
680 matrix. Muscle Nerve. 2011;44(3):318-31.
681 40. Kjaer M. Role of extracellular matrix in adaptation of tendon and skeletal muscle to
682 mechanical loading. Physiol Rev. 2004;84(2):649-98.
683 41. Chemello F, Bean C, Cancellara P, Laveder P, Reggiani C, Lanfranchi G.
684 Microgenomic analysis in skeletal muscle: expression signatures of individual fast and slow
685 myofibers. Plos One. 2011;6(2):e16807.
686 42. De Micheli AJ, Laurilliard EJ, Heinke CL, Ravichandran H, Fraczek P, Soueid-
687 Baumgarten S, et al. Single-Cell Analysis of the Muscle Stem Cell Hierarchy Identifies
688 Heterotypic Communication Signals Involved in Skeletal Muscle Regeneration. Cell Rep.
689 2020;30(10):3583-95 e5.
690 43. Sabatier L, Chen D, Fagotto-Kaufmann C, Hubmacher D, McKee MD, Annis DS, et
691 al. Fibrillin assembly requires fibronectin. Mol Biol Cell. 2009;20(3):846-58.
692 44. Tran PHT, Skrba T, Wondimu E, Galatioto G, Svensson RB, Olesen AT, et al. The
693 influence of fibrillin-1 and physical activity upon tendon tissue morphology and mechanical
694 properties in mice. Physiol Rep. 2019;7(21):e14267.
695 45. Kawasaki BT, Farrar WL. Cancer stem cells, CD200 and immunoevasion. Trends
696 Immunol. 2008;29(10):464-8.
697 46. Draber P, Stepanek O, Hrdinka M, Drobek A, Chmatal L, Mala L, et al. LST1/A is a
698 myeloid leukocyte-specific transmembrane adaptor protein recruiting protein tyrosine
699 phosphatases SHP-1 and SHP-2 to the plasma membrane. J Biol Chem. 2012;287(27):22812-
700 21.
701 47. Ratajczak MZ, Majka M, Kucia M, Drukala J, Pietrzkowski Z, Peiper S, et al.
702 Expression of functional CXCR4 by muscle satellite cells and secretion of SDF-1 by muscle-
703 derived fibroblasts is associated with the presence of both muscle progenitors in bone marrow
704 and hematopoietic stem/progenitor cells in muscles. Stem Cells. 2003;21(3):363-71.
705 48. Sherwood RI, Christensen JL, Conboy IM, Conboy MJ, Rando TA, Weissman IL, et
706 al. Isolation of adult mouse myogenic progenitors: functional heterogeneity of cells within
707 and engrafting skeletal muscle. Cell. 2004;119(4):543-54.
708 49. Farina NH, Hausburg M, Betta ND, Pulliam C, Srivastava D, Cornelison D, et al. A
709 role for RNA post-transcriptional regulation in satellite cell activation. Skelet Muscle.
710 2012;2(1):21.
711 50. Cornelison DD, Filla MS, Stanley HM, Rapraeger AC, Olwin BB. Syndecan-3 and
712 syndecan-4 specifically mark skeletal muscle satellite cells and are implicated in satellite cell
713 maintenance and muscle regeneration. Dev Biol. 2001;239(1):79-94.
714 51. Tanaka KK, Hall JK, Troy AA, Cornelison DD, Majka SM, Olwin BB. Syndecan-4-
715 expressing muscle progenitor cells in the SP engraft as satellite cells during muscle
716 regeneration. Cell Stem Cell. 2009;4(3):217-25.
717 52. Fukada S, Ma Y, Ohtani T, Watanabe Y, Murakami S, Yamaguchi M. Isolation,
718 characterization, and molecular regulation of muscle stem cells. Front Physiol. 2013;4:317.
719 53. Low M, Eisner C, Rossi F. Fibro/Adipogenic Progenitors (FAPs): Isolation by FACS
720 and Culture. Methods Mol Biol. 2017;1556:179-89.

721 54. Kato K, Radbruch A. Isolation and characterization of CD34+ hematopoietic stem
722 cells from human peripheral blood by high-gradient magnetic cell sorting. Cytometry.
723 1993;14(4):384-92.
724 55. Berenson RJ, Andrews RG, Bensinger WI, Kalamasz D, Knitter G, Buckner CD, et al.
725 Antigen CD34+ marrow cells engraft lethally irradiated baboons. J Clin Invest.
726 1988;81(3):951-5.
727 56. Montarras D, Morgan J, Collins C, Relaix F, Zaffran S, Cumano A, et al. Direct
728 isolation of satellite cells for skeletal muscle regeneration. Science. 2005;309(5743):2064-7.
729 57. Heinz S, Romanoski CE, Benner C, Glass CK. The selection and function of cell type-
730 specific enhancers. Nat Rev Mol Cell Biol. 2015;16(3):144-54.
731 58. Andersson R, Gebhard C, Miguel-Escalada I, Hoof I, Bornholdt J, Boyd M, et al. An
732 atlas of active enhancers across human cell types and tissues. Nature. 2014;507(7493):455-61.
733 59. Schiaffino S, Reggiani C. Molecular diversity of myofibrillar proteins: gene regulation
734 and functional significance. Physiol Rev. 1996;76(2):371 - 423.
735 60. Schiaffino S, Reggiani C. Fiber types in mammalian skeletal muscles. Physiol Rev.
736 2011;91(4):1447 - 531.
737 61. Egner IM, Bruusgaard JC, Eftestøl E, Gundersen K. A cellular memory mechanism
738 aids overload hypertrophy in muscle long after an episodic exposure to anabolic steroids. J
739 Physiology. 2013;591(24):6221 - 30.
740 62. Li A, Nelson SR, Rahmanseresht S, Braet F, Cornachione AS, Previs SB, et al.
741 Skeletal MyBP-C isoforms tune the molecular contractility of divergent skeletal muscle
742 systems. Proc Natl Acad Sci U S A. 2019;116(43):21882-92.
743 63. Dhoot GK, Hales MC, Grail BM, Perry SV. The isoforms of C protein and their
744 distribution in mammalian skeletal muscle. J Muscle Res Cell Motil. 1985;6(4):487-505.
745 64. Terry EE, Zhang X, Hoffmann C, Hughes LD, Lewis SA, Li J, et al. Transcriptional
746 profiling reveals extraordinary diversity among skeletal muscle tissues. Elife. 2018;7:1334.
747 65. Berquin A, Lebacq J. Parvalbumin, Labile Heat and Slowing of Relaxation in Mouse
748 Soleus and Extensor Digitorum Longus Muscles. J Physiol-London. 1992;445:601-16.
749 66. Sakakibara I, Santolini M, Ferry A, Hakim V, Maire P. Six homeoproteins and a linc-
750 RNA at the fast MYH locus lock fast myofiber terminal phenotype. Plos Genet.
751 2014;10(5):e1004386.
752 67. Liu L, Ding C, Fu T, Feng Z, Lee JE, Xiao L, et al. Histone methyltransferase MLL4
753 controls myofiber identity and muscle performance through MEF2 interaction. J Clin Invest.
754 2020;130(9):4710-25.
755 68. Davis CA, Hitz BC, Sloan CA, Chan ET, Davidson JM, Gabdank I, et al. The
756 Encyclopedia of DNA elements (ENCODE): data portal update. Nucleic Acids Research.
757 2018;46(D1):D794 - D801.
758 69. Consortium EP. An integrated encyclopedia of DNA elements in the human genome.
759 Nature. 2012;489(7414):57 - 74.
760 70. Neph S, Vierstra J, Stergachis AB, Reynolds AP, Haugen E, Vernot B, et al. An
761 expansive human regulatory lexicon encoded in transcription factor footprints. Nature.
762 2012;489(7414):83 - 90.
763 71. Bergmann O, Zdunek S, Alkass K, Druid H, Bernard S, Frisén J. Identification of
764 cardiomyocyte nuclei and assessment of ploidy for the analysis of cell turnover. Exp Cell Res.
765 2011;317(2):188 - 94.
766 72. Begue G, Raue U, Jemiolo B, Trappe S. DNA methylation assessment from human
767 slow- and fast-twitch skeletal muscle fibers. Journal of applied physiology (Bethesda, Md :
768 1985). 2017;122(4):952 - 67.

769 73. Chemello F, Grespi F, Zulian A, Cancellara P, Hebert-Chatelain E, Martini P, et al.
770 Transcriptomic Analysis of Single Isolated Myofibers Identifies miR-27a-3p and miR-142-3p
771 as Regulators of Metabolism in Skeletal Muscle. Cell Reports. 2019;26(13):3784 - 97.e8.
772 74. Schiaffino S, Reggiani C, Murgia M. Fiber type diversity in skeletal muscle explored
773 by mass spectrometry-based single fiber proteomics. Histol Histopathol. 2020;35(3):239-46.
774 75. Murgia M, Nagaraj N, Deshmukh AS, Zeiler M, Cancellara P, Moretti I, et al. Single
775 muscle fiber proteomics reveals unexpected mitochondrial specialization. 2015;16(3):387-95.
776 76. Vikstrom KL, Seiler SH, Sohn RL, Strauss M, Weiss A, Welikson RE, et al. The
777 vertebrate myosin heavy chain: genetics and assembly properties. Cell Struct Funct.
778 1997;22(1):123-9.
779 77. Peng XL, So KK, He L, Zhao Y, Zhou J, Li Y, et al. MyoD- and FoxO3-mediated
780 hotspot interaction orchestrates super-enhancer activity during myogenic differentiation.
781 Nucleic Acids Res. 2017;45(15):8785-805.
782 78. Adam RC, Yang H, Rockowitz S, Larsen SB, Nikolova M, Oristian DS, et al. Pioneer
783 factors govern super-enhancer dynamics in stem cell plasticity and lineage choice. Nature.
784 2015;521(7552):366-70.
785 79. Whyte WA, Orlando DA, Hnisz D, Abraham BJ, Lin CY, Kagey MH, et al. Master
786 transcription factors and mediator establish super-enhancers at key cell identity genes. Cell.
787 2013;153(2):307-19.
788 80. Parker SC, Stitzel ML, Taylor DL, Orozco JM, Erdos MR, Akiyama JA, et al.
789 Chromatin stretch enhancer states drive cell-specific gene regulation and harbor human
790 disease risk variants. Proc Natl Acad Sci U S A. 2013;110(44):17921-6.
791 81. Rana ZA, Gundersen K, Buonanno A. Activity-dependent repression of muscle genes
792 by NFAT. Proc National Acad Sci. 2008;105(15):5921 - 6.
793 82. Dos Santos M, Backer S, Saintpierre B, Izac B, Andrieu M, Letourneur F, et al.
794 Single-nucleus RNA-seq and FISH identify coordinated transcriptional activity in mammalian
795 myofibers. Nat Commun. 2020;11(1):5102.
796 83. Nylen C, Aoi W, Abdelmoez AM, Lassiter DG, Lundell LS, Wallberg-Henriksson H,
797 et al. IL6 and LIF mRNA expression in skeletal muscle is regulated by AMPK and the
798 transcription factors NFYC, ZBTB14, and SP1. Am J Physiol Endocrinol Metab.
799 2018;315(5):E995-E1004.
800 84. Neph S, Stergachis AB, Reynolds A, Sandstrom R, Borenstein E,
801 Stamatoyannopoulos JA. Circuitry and Dynamics of Human Transcription Factor Regulatory
802 Networks. Cell. 2012;150(6):1274 - 86.
803 85. Rhie SK, Yao L, Luo Z, Witt H, Schreiner S, Guo Y, et al. ZFX acts as a
804 transcriptional activator in multiple types of human tumors by binding downstream of
805 transcription start sites at the majority of CpG island promoters. Genome Res. 2018.
806 86. Hou N, Ye B, Li X, Margulies KB, Xu H, Wang X, et al. Transcription Factor 7-like 2
807 Mediates Canonical Wnt/beta-Catenin Signaling and c-Myc Upregulation in Heart Failure.
808 Circ Heart Fail. 2016;9(6).
809 87. Iyer LM, Nagarajan S, Woelfer M, Schoger E, Khadjeh S, Zafiriou MP, et al. A
810 context-specific cardiac beta-catenin and GATA4 interaction influences TCF7L2 occupancy
811 and remodels chromatin driving disease progression in the adult heart. Nucleic Acids Res.
812 2018;46(6):2850-67.
813 88. Taglietti V, Maroli G, Cermenati S, Monteverde S, Ferrante A, Rossi G, et al. Nfix
814 Induces a Switch in Sox6 Transcriptional Activity to Regulate MyHC-I Expression in Fetal
815 Muscle. Cell Rep. 2016;17(9):2354-66.
816 89. Piette J, Klarsfeld A, Changeux JP. Interaction of nuclear factors with the upstream
817 region of the a-subunit gene of chicken muscle acetylcholine receptor: variations with muscle
818 differentiation and denervation. Embo J. 1989;8(687):687-94.

819 90. Calabria E, Ciciliot S, Moretti I, Garcia M, Picard A, Dyar KA, et al. NFAT isoforms
820 control activity-dependent muscle fiber type specification. Proc National Acad Sci.
821 2009;106(32):13335 - 40.
822 91. Gundersen K. J Exp Biol. 2016;219(2):235 - 42.
823 92. Anderson CM, Hu JX, Barnes RM, Heidt AB, Cornelissen I, Black BL. Myocyte
824 enhancer factor 2C function in skeletal muscle is required for normal growth and glucose
825 metabolism in mice. Skeletal Muscle. 2015;5.
826 93. Potthoff MJ, Wu H, Arnold MA, Shelton JM, Backs J, McAnally J, et al. Histone
827 deacetylase degradation and MEF2 activation promote the formation of slow-twitch
828 myofibers. Journal of Clinical Investigation. 2007;117(9):2459-67.
829 94. Sartorelli V, Huang J, Hamamori Y, Kedes L. Molecular mechanisms of myogenic
830 coactivation by p300: direct interaction with the activation domain of MyoD and with the
831 MADS box of MEF2C. Mol Cell Biol. 1997;17(2):1010-26.
832 95. He J, Ye J, Cai Y, Riquelme C, Liu JO, Liu X, et al. Structure of p300 bound to MEF2
833 on DNA reveals a mechanism of enhanceosome assembly. Nucleic Acids Res.
834 2011;39(10):4464-74.
835 96. Wu H, Rothermel B, Kanatous S, Rosenberg P, Naya FJ, Shelton JM, et al. Activation
836 of MEF2 by muscle activity is mediated through a calcineurin-dependent pathway. Embo J.
837 2001;20(22):6414-23.
838 97. Xu Q, Wu Z. The insulin-like growth factor-phosphatidylinositol 3-kinase-Akt
839 signaling pathway regulates myogenin expression in normal myogenic cells but not in
840 rhabdomyosarcoma-derived RD cells. J Biol Chem. 2000;275(47):36750-7.
841 98. Wu H, Naya FJ, McKinsey TA, Mercer B, Shelton JM, Chin ER, et al. MEF2
842 responds to multiple calcium-regulated signals in the control of skeletal muscle fiber type.
843 Embo J. 2000;19(9):1963-73.
844 99. Wei X, Sun W, Fan R, Hahn J, Joetham A, Li G, et al. MEF2C regulates c-Jun but not
845 TNF-alpha gene expression in stimulated mast cells. Eur J Immunol. 2003;33(10):2903-9.
846 100. McKinsey TA, Zhang CL, Olson EN. MEF2: a calcium-dependent regulator of cell
847 division, differentiation and death. Trends Biochem Sci. 2002;27(1):40-7.
848 101. Potthoff MJ, Olson EN. MEF2: a central regulator of diverse developmental programs.
849 Development. 2007;134(23):4131-40.
850 102. Baskin KK, Makarewich CA, DeLeon SM, Ye W, Chen B, Beetz N, et al. MED12
851 regulates a transcriptional network of calcium-handling genes in the heart. JCI Insight.
852 2017;2(14).
853 103. Burri L, Thoresen GH, Berge RK. The Role of PPARalpha Activation in Liver and
854 Muscle. PPAR Res. 2010;2010.
855 104. Finck BN, Bernal-Mizrachi C, Han DH, Coleman T, Sambandam N, LaRiviere LL, et
856 al. A potential link between muscle peroxisome proliferator- activated receptor-alpha
857 signaling and obesity-related diabetes. Cell Metab. 2005;1(2):133-44.
858 105. Fan W, Evans R. PPARs and ERRs: molecular mediators of mitochondrial
859 metabolism. Current Opinion in Cell Biology. 2015;33:49 - 54.
860 106. Lunde IG, Ekmark M, Rana ZA, Buonanno A, Gundersen K. PPARdelta expression is
861 influenced by muscle activity and induces slow muscle properties in adult rat muscles after
862 somatic gene transfer. J Physiol. 2007;582(Pt 3):1277-87.
863 107. Goldstein I, Baek S, Presman DM, Paakinaho V, Swinstead EE, Hager GL.
864 Transcription factor assisted loading and enhancer dynamics dictate the hepatic fasting
865 response. Genome Res. 2017;27(3):427-39.
866 108. Karam CN, Warren CM, Henze M, Banke NH, Lewandowski ED, Solaro RJ.
867 Peroxisome proliferator-activated receptor-alpha expression induces alterations in cardiac

myofilaments in a pressure-overload model of hypertrophy. American Journal of Physiology-Heart and Circulatory Physiology. 2017;312(4):H681-H90.
109. Gan Z, Rumsey J, Hazen BC, Lai L, Leone TC, Vega RB, et al. Nuclear receptor/microRNA circuitry links muscle fiber type to energy metabolism. J Clin Invest. 2013;123(6):2564-75.
110. Grifone R, Laclef C, Spitz F, Lopez S, Demignon J, Guidotti JE, et al. Six1 and Eya1 expression can reprogram adult muscle from the slow-twitch phenotype into the fast-twitch phenotype. Mol Cell Biol. 2004;24(14):6253-67.
111. Hughes SM, Taylor JM, Tapscott SJ, Gurley CM, Carter WJ, Peterson CA. Selective accumulation of MyoD and myogenin mRNAs in fast and slow adult skeletal muscle is controlled by innervation and hormones. Development. 1993;118(4):1137-47.
112. Li L, Liang Y, Kang L, Liu Y, Gao S, Chen S, et al. Transcriptional Regulation of the Warburg Effect in Cancer by SIX1. Cancer Cell. 2018;33(3):368 - 85.e7.
113. Sakakibara I, Wurmser M, Santos MD, Santolini M, Ducommun S, Davaze R, et al. Six1 homeoprotein drives myofiber type IIA specialization in soleus muscle. Skeletal muscle. 2016;6(1):30.
114. Ekmark M, Rana ZA, Stewart G, Hardie DG, Gundersen K. De-phosphorylation of MyoD is linking nerve-evoked activity to fast myosin heavy chain expression in rodent adult skeletal muscle. J Physiol. 2007;584(Pt 2):637-50.
115. Blum R. Activation of muscle enhancers by MyoD and epigenetic modifiers. J Cell Biochem. 2014;115(11):1855-67.
116. Hernandez-Hernandez JM, Garcia-Gonzalez EG, Brun CE, Rudnicki MA. The myogenic regulatory factors, determinants of muscle development, cell identity and regeneration. Semin Cell Dev Biol. 2017;72:10-8.
117. Puri PL, Avantaggiati ML, Balsano C, Sang N, Graessmann A, Giordano A, et al. p300 is required for MyoD-dependent cell cycle arrest and muscle-specific gene transcription. Embo J. 1997;16(2):369-83.
118. Polesskaya A, Naguibneva I, Duquet A, Bengal E, Robin P, Harel-Bellan A. Interaction between acetylated MyoD and the bromodomain of CBP and/or p300. Mol Cell Biol. 2001;21(16):5312-20.
119. Zhao Y, Zhou J, He L, Li Y, Yuan J, Sun K, et al. MyoD induced enhancer RNA interacts with hnRNPL to activate target gene transcription during myogenic differentiation. Nat Commun. 2019;10(1):5787.
120. Preissl S, Schwaderer M, Raulf A, Hesse M, Gruning BA, Kobele C, et al. Deciphering the Epigenetic Code of Cardiac Myocyte Transcription. Circ Res. 2015;117(5):413-23.
121. Morton JJ, Bird G, Refaeli Y, Jimeno A. Humanized Mouse Xenograft Models: Narrowing the Tumor-Microenvironment Gap. Cancer Res. 2016;76(21):6153-8.
122. Li H, Durbin R. Fast and accurate short read alignment with Burrows-Wheeler transform. Bioinformatics. 2009;25(14):1754-60.
123. Li H, Handsaker B, Wysoker A, Fennell T, Ruan J, Homer N, et al. The Sequence Alignment/Map format and SAMtools. Bioinformatics. 2009;25(16):2078-9.
124. Zhang Y, Lin YH, Johnson TD, Rozek LS, Sartor MA. PePr: a peak-calling prioritization pipeline to identify consistent or differential peaks from replicated ChIP-Seq data. Bioinformatics. 2014;30(18):2568-75.
125. Rodríguez-Castañeda F, Lemma RB, Cuervo I, Bengtsen M, Moen LM, Ledsaak M, et al. The SUMO protease SENP1 and the chromatin remodeler CHD3 interact and jointly affect chromatin accessibility and gene expression. J Biol Chem. 2018;293(40):15439 - 54.
126. Ramírez F, Ryan DP, acids BGN. deepTools2: a next generation web server for deep-sequencing data analysis. academicoupcom.

127. McLean CY, Bristor D, Hiller M, Clarke SL, Schaar BT, Lowe CB, et al. GREAT improves functional interpretation of cis-regulatory regions. Nat Biotechnol. 2010;28(5):495 - 501.
128. Huang da W, Sherman BT, Lempicki RA. Bioinformatics enrichment tools: paths toward the comprehensive functional analysis of large gene lists. Nucleic Acids Res. 2009;37(1):1-13.
129. Huang DW, Sherman BT, Lempicki RA. Systematic and integrative analysis of large gene lists using DAVID bioinformatics resources. Nat Protoc. 2009;4(1):44 - 57.
130. Supek F, Bosnjak M, Skunca N, Smuc T. REVIGO summarizes and visualizes long lists of gene ontology terms. Plos One. 2011;6(7):e21800.
131. Shannon P, Markiel A, Ozier O, Baliga NS, Wang JT, Ramage D, et al. Cytoscape: a software environment for integrated models of biomolecular interaction networks. Genome Res. 2003;13(11):2498 - 504.
132. McLeay RC, Bailey TL. Motif Enrichment Analysis: a unified framework and an evaluation on ChIP data. Bmc Bioinformatics. 2010;11(1):1 - 11.

935

936

937

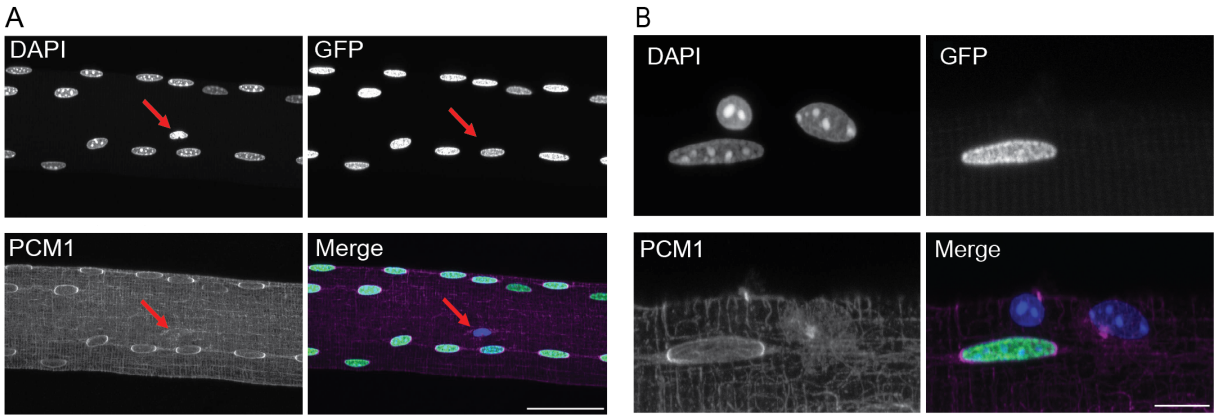

938

939 **Fig. 1**

940

941

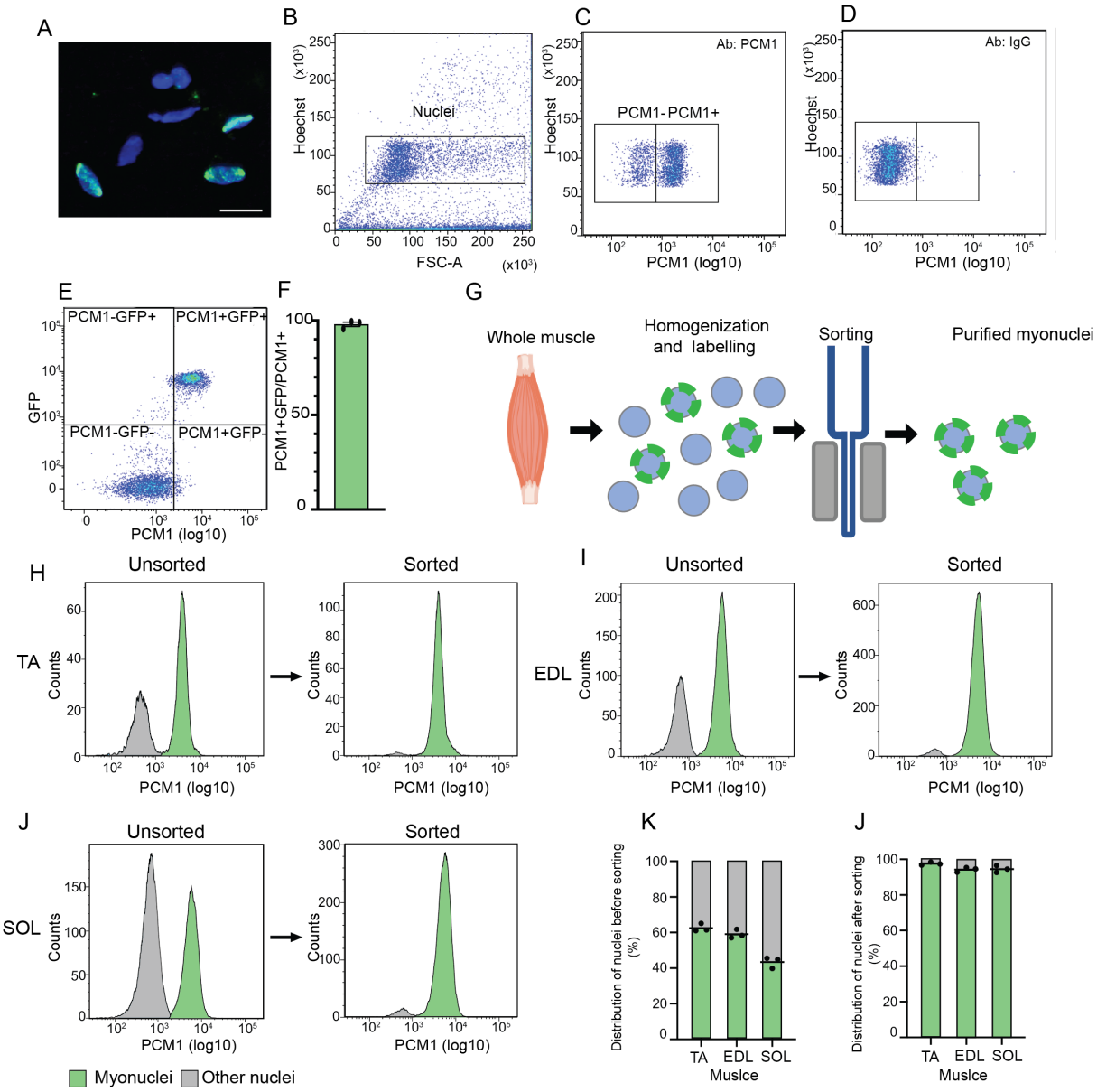

942

943 **Fig. 2**

944

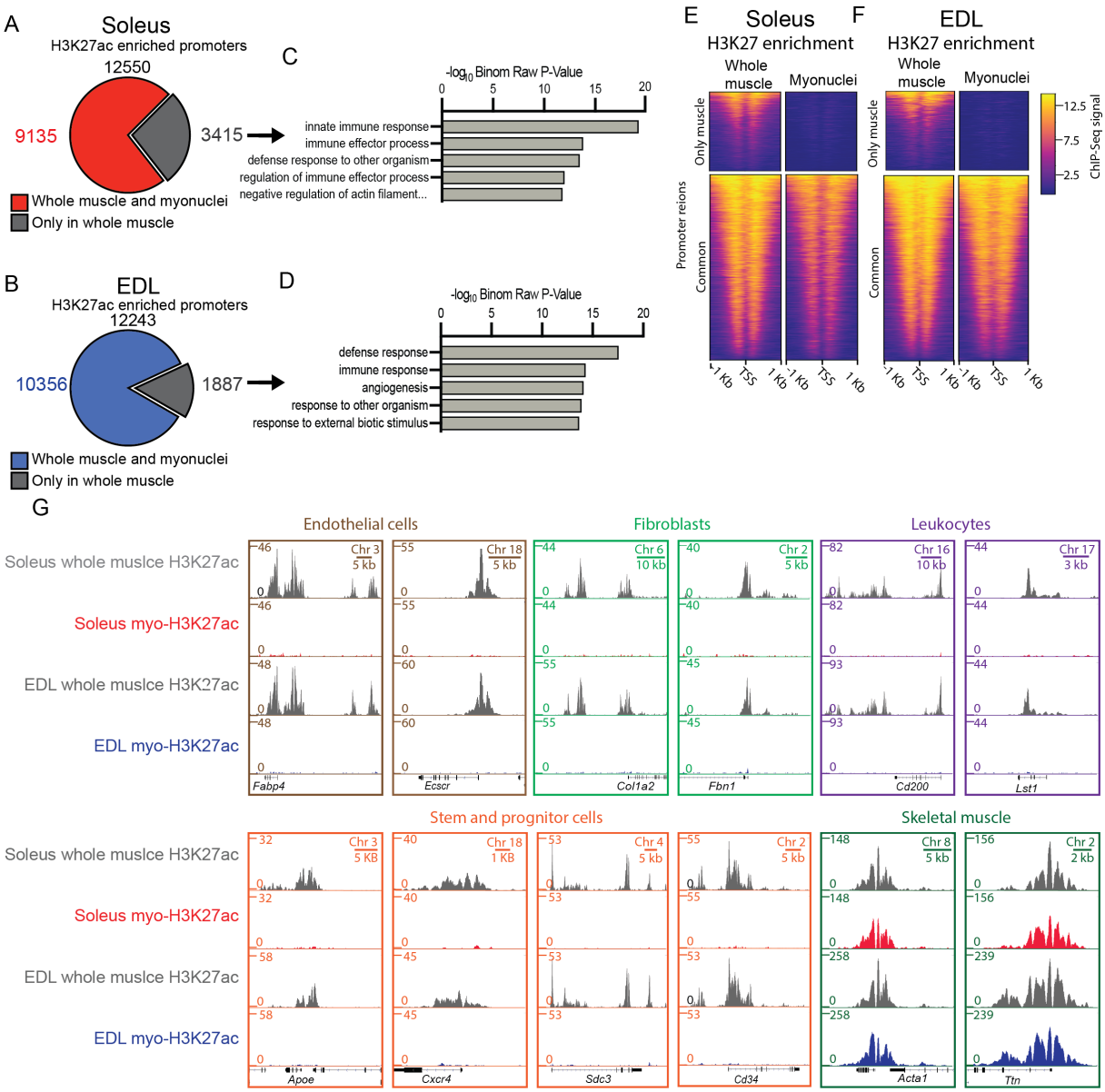

Fig. 3

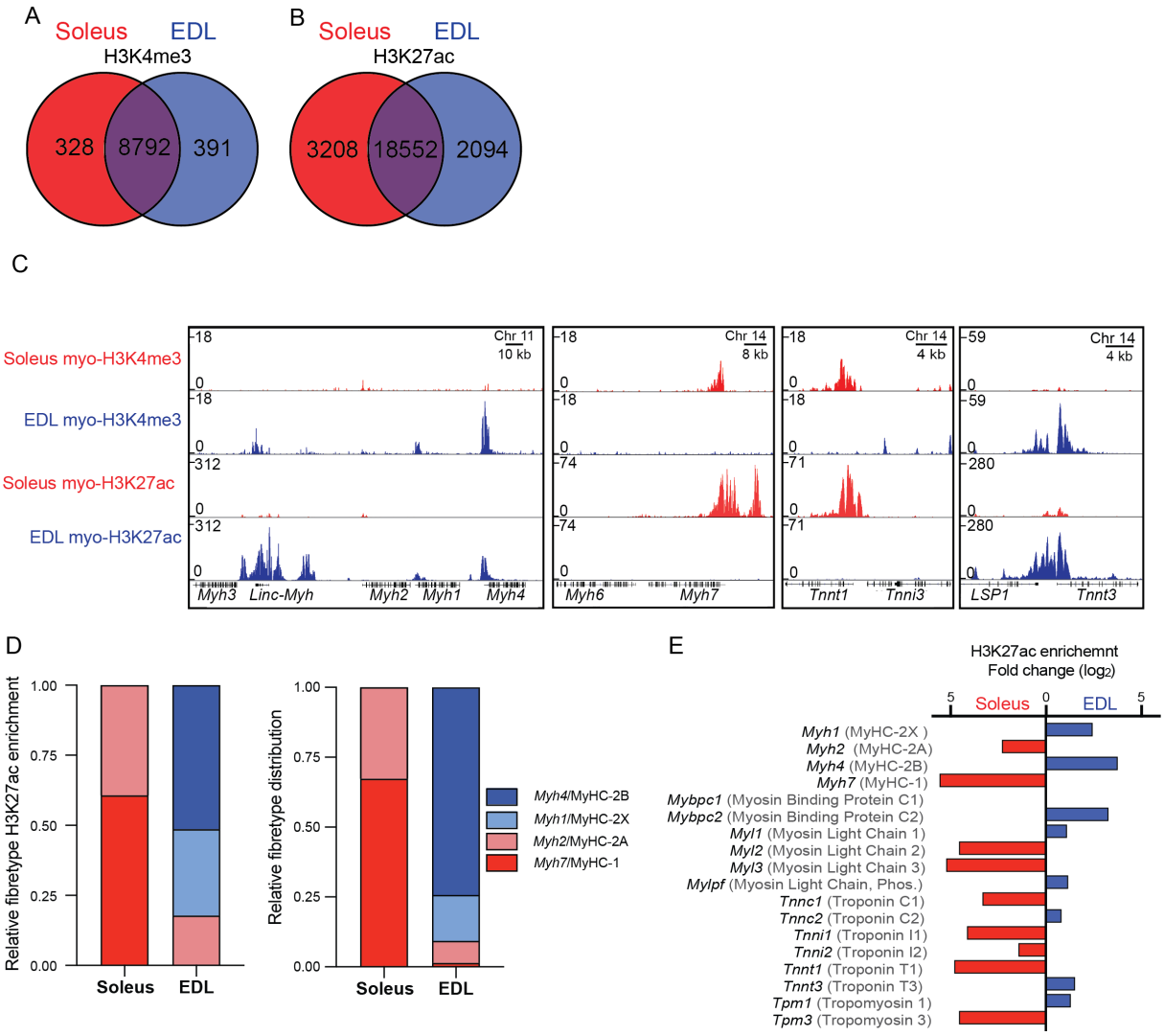

Fig. 4

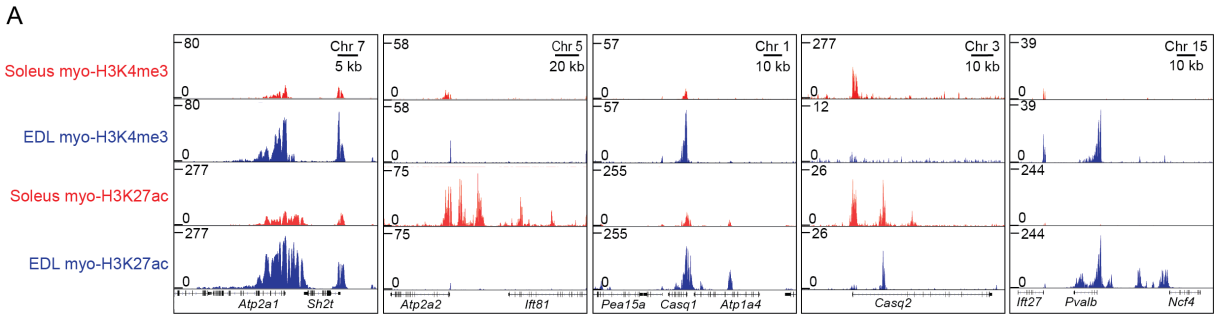

Fig. 5

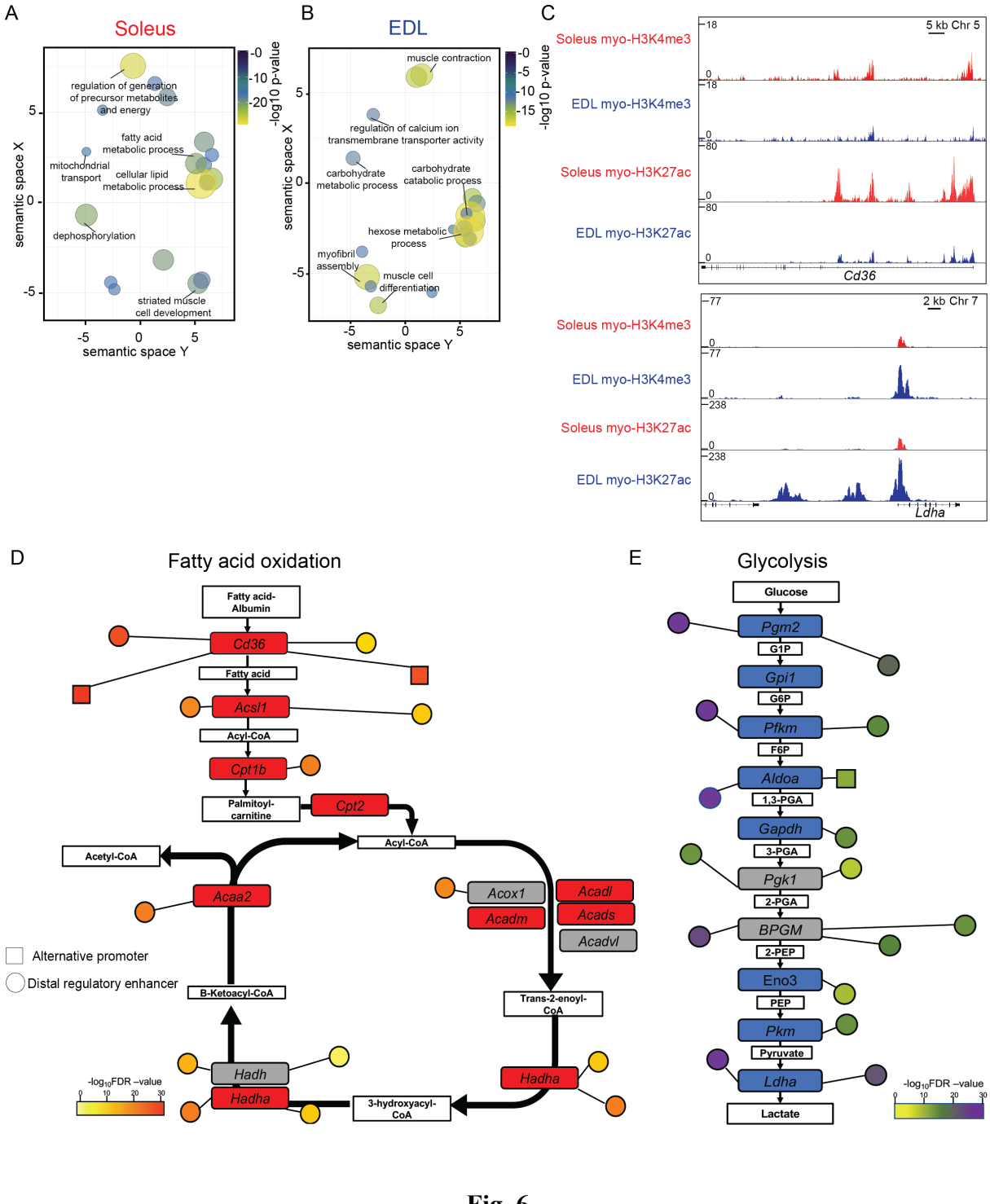

Fig. 6

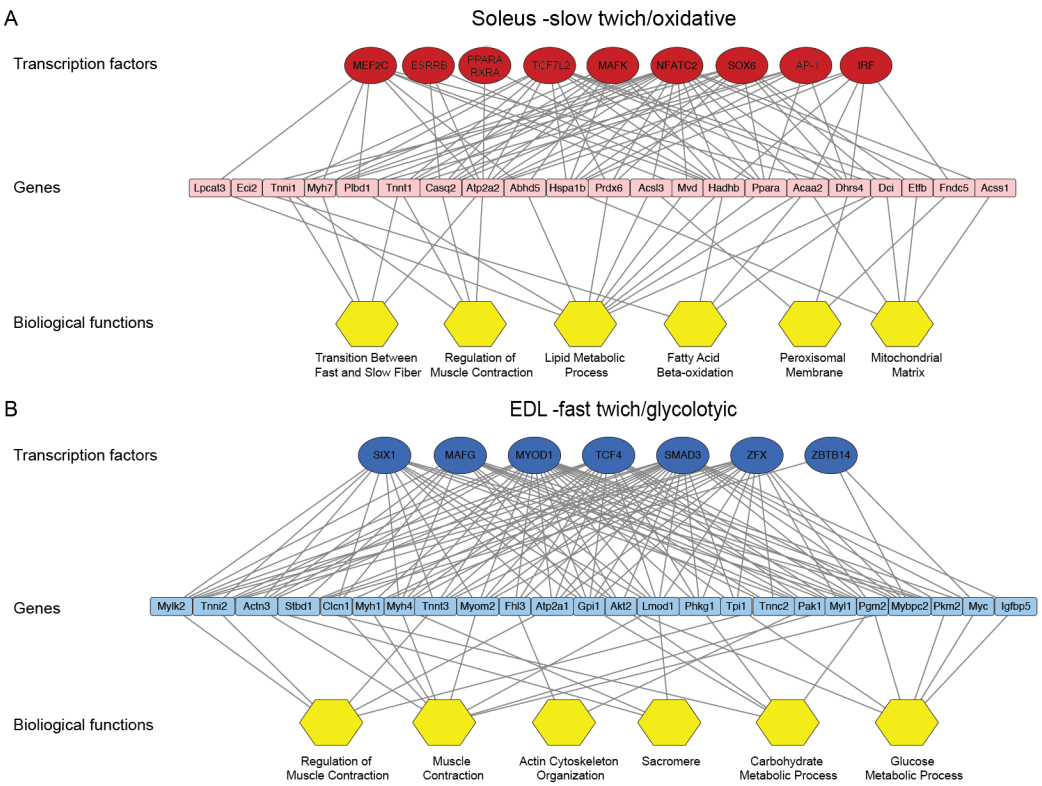

Fig. 7